

Relativistic time transfer for a Mars lander: from proper time to Areocentric Coordinate Time

De-Wang Xu, Qing-Shan Yu and Yi Xie

School of Astronomy and Space Science, Nanjing University, Nanjing 210093, China; yixie@nju.edu.cn
Shanghai Key Laboratory of Space Navigation and Position Techniques, Shanghai 200030, China
Key Laboratory of Modern Astronomy and Astrophysics, Nanjing University, Ministry of Education, Nanjing 210093, China

Received 2016 May 24; accepted 2016 June 9

Abstract As the first step in relativistic time transfer for a Mars lander from its proper time to the time scale at the ground station, we investigate the transformation between proper time and Areocentric Coordinate Time (TCA) in the framework of IAU Resolutions. TCA is a local time scale for Mars, which is analogous to the Geocentric Coordinate Time (TCG) for Earth. This transformation contains two contributions: internal and external. The internal contribution comes from the gravitational potential and the rotation of Mars. The external contribution is due to the gravitational fields of other bodies (except Mars) in the Solar System. When the (in)stability of an onboard clock is assumed to be at the level of 10^{-13} , we find that the internal contribution is dominated by the gravitational potential of spherical Mars with necessary corrections associated with the height of the lander on the areoid, the dynamic form factor of Mars, the flattening of the areoid and the spin rate of Mars. For the external contribution, we find the gravitational effects from other bodies in the Solar System can be safely neglected in this case after calculating their maximum values.

Key words: reference systems — time — space vehicles

1 INTRODUCTION

For deep space missions, synchronization between the clock onboard a space vehicle and a clock on the ground plays a crucial role in control, navigation and scientific operation. In such a procedure of time transfer, Einstein's general relativity (GR) has "long since passed from the realm of theoretical physics to the realm of engineering design" (Nelson 2011). It is worth mentioning that we are now in the centenary of GR (e.g. Iorio 2015). According to the principles of GR, different kinds of times, which are proper times and coordinate times, should be used in order to replace Newton's absolute time (Misner et al. 1973; Landau & Lifshitz 1975).

The proper time τ is defined by the readings of an ideal clock. τ is an observable and is only associated with the clock itself. Nevertheless, an atomic clock, which is widely used on the ground and in space, departs from the ideal case. The coordinate times cannot be measured directly, but they might be used as variables in the equations of motion of celestial and artificial bodies and light rays. The coordinate times are connected with the proper time through a four-dimensional spacetime interval, which significantly changes the method used for clock synchronization and time transfer (Petit & Wolf 2005; Nelson 2007, 2011). Experiments involving time/frequency transfer might also

be used for testing theories of gravity (Samain 2002; Cacciapuoti & Salomon 2009; Wolf et al. 2009; Christophe et al. 2009; Schiller et al. 2009; Christophe et al. 2012; Deng & Xie 2013a,b, 2014; Zhang et al. 2014; Xie & Huang 2015; Hees et al. 2014; Angélil et al. 2014; Delva et al. 2015; Deng 2016). There are other performed or proposed tests of GR and non-Newtonian gravity that use existing or proposed orbiters (Iorio 2006, 2009, 2010; Turyshev et al. 2010; Le Poncin-Lafitte 2011; Dirx et al. 2016; Oberst et al. 2012).

Relativistic time transfers in various contexts, such as in the vicinity of Earth (Klioner 1992; Petit & Wolf 1994; Wolf & Petit 1995; Petit & Wolf 1997; Kouba 2002, 2004; Petit & Wolf 2005; Nelson 2007, 2011; Xie 2016) and in the Solar System (Nelson 2007; Minazzoli & Chauvineau 2009; Nelson 2011; Deng 2012; Hees et al. 2012; Pan & Xie 2013, 2014, 2015; Deng 2015; Dirx et al. 2015, 2016), have been intensively studied and discussed. In those contexts, one clock is onboard a satellite or an orbiter and the other one is on the ground. In the present and following works, we will consider the time transfer from a Mars lander to a ground clock and discuss its algorithm for computation, where the relativistic effects are fully taken into account.

In the procedure of time transfer for a Mars lander, some reference systems and time scales are needed

in light of the International Astronomical Union (IAU) 2000 Resolutions for general relativistic reference systems (Soffel et al. 2003). The lander is locally in the gravitational field of Mars so that the Areocentric Celestial Reference System (ACRS) has to be introduced to describe the motion and transmission of signals by the lander. The time coordinate of the ACRS is the Areocentric Coordinate Time (TCA). The ACRS and the TCA are respectively analogous to the Geocentric Celestial Reference System (GCRS) and the Geocentric Coordinate Time (TCG) (Soffel et al. 2003), which are used to characterize events that happen in the vicinity of Earth. In order to connect these two local reference systems, we need a global reference system, the Solar System Barycentric Celestial Reference System (BCRS), and its time coordinate, the Barycentric Coordinate Time (TCB), which can be used to model light propagation and the motion of bodies in the Solar System (Soffel et al. 2003). According to IAU 2006 Resolution B2¹, the BCRS is assumed to be oriented according to the International Celestial Reference System (ICRS) axes and the orientation of the GCRS is derived from the ICRS-oriented BCRS. Following this resolution, we also define that the orientation of the ACRS is derived from the ICRS-oriented BCRS and the ACRS is kinematically nonrotating with respect to the BCRS. It means that the orientation of the ACRS is the same as that of the ICRS (BCRS).

For such a relativistic time transfer from the lander to the ground station, several steps are involved:

- (1) Transformation from the proper time τ of the clock onboard a Mars lander to TCA;
- (2) Transformation from TCA to TCB;
- (3) Transformation from TCB to TCG;
- (4) Transformation from TCG to the time scale of a clock on the ground;
- (5) Take the flight time of light into account for synchronization of the clocks.

Steps 3 and 4 are well known and the standard procedures under the framework of IAU 2000 Resolutions can be found in Soffel et al. (2003) and references therein. In this investigation, we will focus on step 1, which is related to the transformation from τ to TCA. Steps 2 and 5 will be left to our future works.

In addition to the principles of GR, limits of current and near future techniques also have to be taken into account. One main factor is (in)stability of the onboard clock. In the case of the two Voyager missions, the phase stability of their onboard ultrastable oscillators (USOs) is $\sigma_y = 5 \times 10^{-12}$ at a 1 s time interval for Allan deviation (Marouf et al. 1986). Cassini's USO is over ten times better than Voyager's with an Allan deviation of $\sigma_y = 2 \times 10^{-13}$ at 1 s (Kliore et al. 2004). The New Horizons spacecraft carries two USOs, each of which is an ovenized crystal oscillator. Its short-term frequency stability σ_y at 1-second and 10-second intervals is respectively better than 3×10^{-13} and

2×10^{-13} (Fountain et al. 2008). Based on these technical facts, we assume that the stability of the clock onboard the Mars lander, which we consider in our investigation, is at the level of 10^{-13} and we will neglect all contributions smaller than this threshold.

The rest of this paper is organized as follows. Section 2 is devoted to modeling the time transfer between τ and TCA. This transformation has two parts: internal and external contributions, which will be respectively examined in Sections 3 and 4. Finally, in Section 5, we summarize our results.

2 TRANSFORMATION BETWEEN τ AND TCA

In the framework of IAU 2000 Resolutions (Soffel et al. 2003), the ACRS needs to be constructed to describe events in the vicinity of Mars and it has its own time coordinate TCA. The underlying principles for such a construction and the mathematical description of the reference system are very similar to those of the GCRS and TCG (Soffel et al. 2003). Following the standard procedure for time transfer (Wolf & Petit 1995; Petit & Wolf 1997), we can describe the transformation between the proper time τ of the clock onboard a Mars lander and TCA, $T_{\mathcal{O}}$, as

$$\frac{d\tau}{dT_{\mathcal{O}}} = 1 - \epsilon^2(F_{\mathcal{O}} + \bar{F}_{\mathcal{O}}) + \mathcal{O}(\epsilon^4), \quad (1)$$

where the internal contribution $F_{\mathcal{O}}$ and external one $\bar{F}_{\mathcal{O}}$ are

$$F_{\mathcal{O}} = U_{\mathcal{O}}(\mathbf{X}) + \frac{1}{2}\mathbf{V}^2, \quad (2)$$

$$\bar{F}_{\mathcal{O}} = \bar{U}_{\mathcal{O}}(\mathbf{x}_{\mathcal{O}} + \mathbf{X}) - \bar{U}_{\mathcal{O}}(\mathbf{x}_{\mathcal{O}}) - \mathbf{X} \cdot \nabla \bar{U}_{\mathcal{O}}(\mathbf{x}_{\mathcal{O}}) + \mathbf{X} \cdot \mathbf{Q}_{\mathcal{O}}. \quad (3)$$

Here, $\epsilon = c^{-1}$ and c is the speed of light; $U_{\mathcal{O}}(\mathbf{X})$ is the Newtonian gravitational potential of Mars evaluated at the position of the lander, \mathbf{X} ; \mathbf{V} is the velocity of the lander in the ACRS; $\bar{U}_{\mathcal{O}}(\mathbf{x})$ is the Newtonian gravitational potential of external masses (except Mars) evaluated at the coordinate \mathbf{x} ; $\mathbf{x}_{\mathcal{O}}$ is the coordinate of the areocenter in the BCRS; the $\mathbf{Q}_{\mathcal{O}}$ term is related to the 4-acceleration of the areocenter in the external gravitational field due to its mass quadrupole.

For the internal contribution (2), $F_{\mathcal{O}}$ depends on the gravitational potential of Mars $U_{\mathcal{O}}$. Mars is not a spherically symmetric body in the gravitational and geometric senses. For the gravitational potential of Mars, its deviation from the potential of a point mass can be characterized by the coefficients of the spherical harmonic expansion of $U_{\mathcal{O}}$. For the geometric position of an event close to Mars' surface, the deviation from a spherical body will make its areodetic coordinates different from its areocentric ones, which can be described by the flattening of the areoid. $F_{\mathcal{O}}$ also depends on the local velocity of the lander \mathbf{V} . If we assume the lander stays at its landing site without any motion, its velocity is mainly determined by the

¹ https://www.iau.org/static/resolutions/IAU2006_Resol2.pdf

diurnal rotation of Mars. The velocity has small additional contributions from precession, nutation and the change in obliquity of Mars. Although the high-order non-spherical parts of the gravitational potential and the areoid of Mars are believed to be small and might be neglected, a detailed assessment is required. This is also true for the small contributions from the velocity of the lander; see Section 3 for a detailed investigation.

For the external contribution (3) in the time transfer, \bar{F}_{σ} depends on the gravitational fields of the external bodies. It was shown by Wolf & Petit (1995) that, in the case of time transfer for a satellite around Earth at height 3×10^5 km, the contributions of the Moon, Sun and Venus can be greater than the level of 10^{-18} . It was also found (Kouba 2004) that, at a pico-second (ps) precision level or an inaccuracy in frequency of 10^{-16} , the effects of external masses can be neglected in the time transfer associated with the Global Positioning System (GPS). In Section 4, we will calculate the effects of the Sun, other planets, Pluto, the three most massive asteroids and the Martian satellites on the external part of time transfer \bar{F}_{σ} .

3 INTERNAL CONTRIBUTION TO TIME TRANSFER

The internal contribution can further be divided into two parts: the gravitational potential of Mars and the local velocity of the lander. If the lander is static with respect to Mars' surface, then its local velocity is totally determined by the rotation of Mars, including the diurnal changes, precession, nutation and the change in obliquity of Mars.

3.1 Gravitational Potential of Mars

The gravitational potential of Mars U_{σ} can be represented as a spherical harmonic expansion, which reads as (e.g. Torge 1991; Hofmann-Wellenhof & Moritz 2005)

$$U_{\sigma} = \frac{GM_{\sigma}}{R} + \frac{GM_{\sigma}}{R} \sum_{n=2}^{\infty} \sum_{m=0}^{\infty} \left(\frac{R_e}{R} \right)^n \times \bar{P}_{nm}(\sin \varphi) \times [\bar{C}_{nm} \cos(m\lambda) + \bar{S}_{nm} \sin(m\lambda)]. \quad (4)$$

Here, GM_{σ} is the gravitational constant times the mass of Mars; n is the degree, m is the order, \bar{P}_{nm} are the fully normalized associated Legendre polynomials; \bar{C}_{nm} and \bar{S}_{nm} are dimensionless Stokes coefficients which are fully normalized; φ is the areocentric latitude, and λ is the longitude (east positive); R_e is the reference radius of a spherical Mars; and $R = |\mathbf{X}|$ is the areocentric distance. The fully normalized associated Legendre functions \bar{P}_{nm} can be computed from the conventional associated Legendre functions P_{nm} by (Torge 1991)

$$\bar{P}_{nm} = \sqrt{k(2n+1) \frac{(n-m)!}{(n+m)!}} P_{nm}, \quad (5)$$

where $k = \begin{cases} 1 & \text{for } m = 0 \\ 2 & \text{for } m \neq 0 \end{cases}$.

In this work, the numerical values of the Stokes coefficients are taken from the Goddard Mars Model 3 (GMM-3) (Genova et al. 2015, 2016a,b), which was recently released and provides the static gravity field of Mars in spherical harmonics. It was calculated using the Deep Space Network tracking data of the NASA Mars missions: Mars Global Surveyor (MGS), Mars Odyssey (ODY) and the Mars Reconnaissance Orbiter (MRO). GMM-3 shows improved correlations with Mars topography up to 15% larger at higher harmonics than previous solutions.

Table 1 lists the parameters and the leading Stokes coefficients of GMM-3 (Genova et al. 2016b); Table 2 shows the parameters of the areoid derived from GMM-3 (Genova et al. 2016b). The whole data set of GMM-3 can be accessed from the Planetary Data System (PDS) Geosciences Node ².

Since the lander is on the surface of Mars, its R is very close to the semi-major axis of the areoid a so that we define two quantities to evaluate contributions of the leading Stokes coefficients in Table 1:

$$\mathfrak{U}_{\bar{C}_{nm}} \equiv \frac{GM_{\sigma}}{c^2 a} \bar{P}_{nm}(\sin \varphi) \bar{C}_{nm} \cos(m\lambda), \quad (6)$$

$$\mathfrak{U}_{\bar{S}_{nm}} \equiv \frac{GM_{\sigma}}{c^2 a} \bar{P}_{nm}(\sin \varphi) \bar{S}_{nm} \sin(m\lambda), \quad (7)$$

where, based on the quantities given in Tables 1 and 2, we use the relation that $R_e = a$ and we can have

$$\frac{GM_{\sigma}}{c^2 a} = 1.40320941 \times 10^{-10}. \quad (8)$$

Table 3 shows the contributions of the leading Stokes coefficients. It can be easily found that only the contribution of \bar{C}_{20} in the time transfer can be larger than the threshold of 10^{-13} .

More specifically, the position of the lander can be conventionally characterized by the areodetic coordinates: the longitude λ , the areodetic latitude φ_g and the areodetic height h with respect to the areoid. When the flattening f of the areoid is taken into account, it is well known that (Torge 1991; Hofmann-Wellenhof & Moritz 2005; Kovalevsky & Seidelmann 2004)

$$R^2 = a^2 \left\{ \left(C + \frac{h}{a} \right)^2 \cos^2 \varphi_g + \left[C(1-f)^2 + \frac{h}{a} \right]^2 \sin^2 \varphi_g \right\}, \quad (9)$$

where the areocentric latitude φ is related to the areodetic latitude φ_g by $\tan \varphi = (1-f)^2 \tan \varphi_g$, and the intermediate function C is

$$C = \left[\cos^2 \varphi_g + (1-f)^2 \sin^2 \varphi_g \right]^{-1/2}. \quad (10)$$

Considering that the flattening f is about 5×10^{-3} (see Table 2), we can safely ignore the Stokes coefficients

² http://pds-geosciences.wustl.edu/mro/mro-m-rss-5-sdp-v1/mrors_1xxx/

Table 1 Parameters and Leading Stokes Coefficients of GMM-3

Parameter	Value
Reference radius R_e	3.3960×10^6 m
Gravitational constant times mass GM_σ	$4.2828372854187757 \times 10^{13}$ m ³ s ⁻²
Dynamic form factor $J_2 \equiv -\sqrt{5}\bar{C}_{20}$	$1.9566067336935673 \times 10^{-3}$
Stokes coefficient \bar{C}_{20}	$-8.7502113235452894 \times 10^{-4}$
Stokes coefficient \bar{C}_{21}	$5.9031495993080755 \times 10^{-10}$
Stokes coefficient \bar{S}_{21}	$-4.9433617424482412 \times 10^{-11}$
Stokes coefficient \bar{C}_{22}	$-8.4635903869414677 \times 10^{-5}$
Stokes coefficient \bar{S}_{22}	$4.8934625860229178 \times 10^{-5}$
Stokes coefficient \bar{C}_{30}	$-1.1896034897013901 \times 10^{-5}$
Stokes coefficient \bar{C}_{40}	$5.1294072971513378 \times 10^{-6}$
Stokes coefficient \bar{C}_{50}	$-1.7266823981571990 \times 10^{-6}$

Notes: The complete set of Stokes coefficients associated with GMM-3 can be accessed from the PDS Geosciences Node.

Table 2 Areoid Derived from GMM-3

Parameter	Value
Semi-major axis a	3.3960×10^6 m
1/Flattening $1/f$	196.877360
Rotation rate ω	$7.088218066303858 \times 10^{-5}$ rad s ⁻¹

Notes: A digital map of the areoid can be accessed from the PDS Geosciences Node.

Table 3 Contributions of the Leading Stokes Coefficients $\mathfrak{U}_{\bar{C}_{nm}}$ and $\mathfrak{U}_{\bar{S}_{nm}}$

Contribution	Min	Max
$\mathfrak{U}_{\bar{C}_{20}}$	-2.74553×10^{-13}	1.37276×10^{-13}
$\mathfrak{U}_{\bar{C}_{21}}$	-1.60406×10^{-19}	1.60406×10^{-19}
$\mathfrak{U}_{\bar{S}_{21}}$	-1.34326×10^{-20}	1.34326×10^{-20}
$\mathfrak{U}_{\bar{C}_{22}}$	-2.29981×10^{-14}	2.29981×10^{-14}
$\mathfrak{U}_{\bar{S}_{22}}$	-1.32970×10^{-14}	1.32970×10^{-14}
$\mathfrak{U}_{\bar{C}_{30}}$	-4.41645×10^{-15}	4.41645×10^{-15}
$\mathfrak{U}_{\bar{C}_{40}}$	-9.25410×10^{-16}	2.15929×10^{-15}
$\mathfrak{U}_{\bar{C}_{50}}$	-8.03584×10^{-16}	8.03584×10^{-16}

beyond \bar{C}_{20} and keep f to its linear order for a time transfer accuracy of 10^{-13} so that

$$U_\sigma \approx \frac{GM_\sigma}{a} \left[1 - \frac{h}{a} + \frac{1}{2} J_2 (1 - 3 \sin^2 \varphi_g) + f \sin^2 \varphi_g \right], \quad (11)$$

where J_2 is the dynamic form factor of Mars and $J_2 \equiv -\sqrt{5}\bar{C}_{20}$. We also assume that $h/a \sim J_2 \sim f$, which means h can range between $\pm 1.7 \times 10^4$ m.

The spherical harmonic expansion (4) and the above calculations refer to the Mars-fixed reference frame whose $X' - Y'$ plane coincides with the true equator of Mars and the Z' axis points along the planet's symmetry axis. This Mars-fixed reference frame is connected to ACRS by the rotation model of Mars, which will be discussed in the next subsection. Areocentric distances remain invariant in these two reference systems. However, real data processing should be performed in a coordinate system like ICRS by employing the Earth's equator at a reference epoch. Thus, in principle, more general formulae should be adopted and developed. This has been done partially so far for orbiting

bodies (Iorio et al. 2011; Renzetti 2013, 2014a). Following these works, we can estimate the effect of departure from alignment of Mars' rotation axis with the coordinate axis Z' by replacing φ_g with $\arccos(\hat{\mathbf{k}} \cdot \hat{\mathbf{R}})$, where $\hat{\mathbf{k}}$ is the unit vector representing the rotation axis of Mars, which is not aligned along the Z' axis. The leading contribution makes Equation (11) independent of the areodetic latitude but keeps the numerical values unchanged. Furthermore, the even zonal multipoles also have an impact in tests of relativistic gravity with orbiters (Iorio et al. 2011, 2013; Renzetti 2014b, 2015).

3.2 Rotation of Mars

Since the lander is assumed to be static with respect to the surface of Mars, its local velocity is determined by the rotation of Mars, which is described by the relation between the Mars-fixed reference system and the ACRS. The Mars-fixed reference system adopted in GMM-3 (Genova et al. 2016b) is described by Konopliv et al. (2006). The prime meridian of the Mars-fixed coordinate is chosen so that it

matches the prime meridian of the IAU 2000 coordinate system to about 20 cm. The rotation from Mars body-fixed position \mathbf{X}' to the ICRS (ACRS) position \mathbf{X} is (Konopliv et al. 2006)

$$\mathbf{X} = R_z(-N)R_x(-J)R_z(-\psi)R_x(-I)R_z(-\phi)\mathbf{X}', \quad (12)$$

where the angle N is from the vernal equinox (node of the mean ecliptic plane or Earth mean orbit of J2000 and the ICRS $x - y$ plane) to the node of the Mars mean orbit and ICRS $x - y$ plane; J is the inclination of Mars' mean orbit relative to the ICRS $x - y$ plane; ψ is the angle from the node of Mars' mean orbit and the ICRS $x - y$ plane to the node of Mars' true equator of date and Mars' mean orbit; I is the inclination of Mars' true equator of date relative to Mars' mean orbit; ϕ is the spin angle from the node of Mars' true equator of date and Mars' mean orbit to the prime meridian of Mars. It is worth mentioning that the Barycentric Dynamical Time (TDB) is usually taken as the time coordinate in the rotational elements for planets and satellites in the Solar System, such as in the report of the IAU Working Group on Cartographic Coordinates and Rotational Elements (Archinal et al. 2011). Theoretically, TDB has a different rate than TCA.

Like the fact that the orientation and rotation of the Earth is changing due to its precession, nutation and obliquity, the angles ψ and I are also directly affected by the nutation of Mars. According to the rotation model of Mars given by Konopliv et al. (2006), we can have

$$\begin{aligned} \psi(T) &= \psi_0 + \dot{\psi}_0 T + \psi_{\text{nut}}, \\ I(T) &= I_0 + \dot{I}_0 T + I_{\text{nut}}, \end{aligned} \quad (13)$$

where T is the time past the J2000 epoch in TDB and the overdot means derivative with respect to T ; the terms ψ_{nut} and I_{nut} are the nutation corrections of Mars; ψ_0 and I_0 are constant angle values at the J2000 epoch, $\dot{\psi}_0$ is a constant that equals the precession rate for Mars, and \dot{I}_0 is a constant equal to the secular change in the obliquity of Mars (orbit inclination) relative to the mean orbit of Mars. The nutation corrections in longitude and obliquity are given by (Reasenberg & King 1979)

$$\psi_{\text{nut}} = \sum_m \psi_m \sin(\alpha_m T + \theta_m), \quad (14)$$

$$I_{\text{nut}} = I_{00} + \sum_m I_m \sin(\alpha_m T + \theta_m), \quad (15)$$

where I_{00} is a small constant correction to the nutation in obliquity, α_m is related to the mean motion of Mars, and θ_m is associated with the mean anomaly of Mars and the argument of perihelion of the Mars orbit relative to the node defined by Mars' equator and its mean orbit. Finally, the spin angle ϕ is defined as (Reasenberg & King 1979)

$$\phi(T) = \phi_0 + \dot{\phi}_0 T - \psi_{\text{nut}} \cos I, \quad (16)$$

where ϕ_0 is the constant value at epoch J2000 and $\dot{\phi}_0$ is the spin rate of Mars. Values of the orientation angles

mentioned above are taken from the currently released MRO120D solution (Konopliv et al. 2016) and are listed in Table 4. It is obvious that the spin rate is much bigger than the precession rate and the secular change of obliquity, i.e.,

$$|\dot{\phi}_0| \gg |\dot{\psi}_0| \gg |\dot{I}_0|. \quad (17)$$

With the rotation model of Mars (12), we can obtain the velocity of the lander in the ACRS as

$$\mathbf{V} \equiv \frac{d\mathbf{X}}{dT} = -(\dot{\phi}_0 R_\phi + \dot{\psi}_0 R_\psi + \dot{I}_0 R_I)\mathbf{X}', \quad (18)$$

where $\mathbf{X}' \equiv (X', Y', Z')^T$ is the position of the lander in the Mars-fixed reference system; the quantities R_ϕ , R_ψ and R_I are defined as

$$R_\phi \equiv R_z(-N)R_x(-J)R_z(-\psi)R_x(-I)\mathcal{D}(R_z)(-\phi), \quad (19)$$

$$R_\psi \equiv R_z(-N)R_x(-J)\mathcal{D}(R_z)(-\psi)R_x(-I)R_z(-\phi), \quad (20)$$

$$R_I \equiv R_z(-N)R_x(-J)R_z(-\psi)\mathcal{D}(R_x)(-I)R_z(-\phi), \quad (21)$$

and the operator \mathcal{D} is defined as

$$\mathcal{D}(R_a)(A) \equiv \left. \frac{d}{d\theta} R_a(\theta) \right|_{\theta=A}, \quad a = x, y, z. \quad (22)$$

Therefore, we can further have that

$$\begin{aligned} \mathbf{V}^2 &= \mathbf{V}_{\dot{\phi}_0}^2 + \mathbf{V}_{\dot{\phi}_0 \dot{\psi}_0}^2 + \mathbf{V}_{\dot{\phi}_0 \dot{I}_0}^2 \\ &+ \mathcal{O}(\dot{\psi}_0^2, \dot{I}_0^2, \dot{\psi}_0 \dot{I}_0, \dot{\phi}_0^3, \dot{\phi}_0^2 \dot{\psi}_0, \dot{\phi}_0^2 \dot{I}_0), \end{aligned} \quad (23)$$

where only the leading terms containing the spin rate $\dot{\phi}_0$ are kept and they are

$$\mathbf{V}_{\dot{\phi}_0}^2 = \dot{\phi}_0^2 (X'^2 + Y'^2), \quad (24)$$

$$\begin{aligned} \mathbf{V}_{\dot{\phi}_0 \dot{\psi}_0}^2 &= 2\dot{\phi}_0 \dot{\psi}_0 (\cos I_0 X'^2 - \sin I_0 \sin \phi_0 X' Z' \\ &+ \cos I_0 Y'^2 - \sin I_0 \cos \phi_0 Y' Z'), \end{aligned} \quad (25)$$

$$\mathbf{V}_{\dot{\phi}_0 \dot{I}_0}^2 = 2\dot{\phi}_0 \dot{I}_0 (-\cos \phi_0 X' + \sin \phi_0 Y') Z'. \quad (26)$$

Here, $\mathbf{V}_{\dot{\phi}_0}^2$ is the pure contribution from the spin rate of Mars; $\mathbf{V}_{\dot{\phi}_0 \dot{\psi}_0}^2$ comes from the coupling between the spin rate and the precession rate; and $\mathbf{V}_{\dot{\phi}_0 \dot{I}_0}^2$ is the coupling between the spin rate and the secular change of obliquity. Before detailed calculation, it can be expected that $|\mathbf{V}_{\dot{\phi}_0}^2| \gg |\mathbf{V}_{\dot{\phi}_0 \dot{\psi}_0}^2| \gg |\mathbf{V}_{\dot{\phi}_0 \dot{I}_0}^2|$. Considering the flattening of the areoid that gives (Torge 1991; Hofmann-Wellenhof & Moritz 2005; Kovalevsky & Seidelmann 2004)

$$X' = a \left(C + \frac{h}{a} \right) \cos \varphi_g \cos \lambda, \quad (27)$$

$$Y' = a \left(C + \frac{h}{a} \right) \cos \varphi_g \sin \lambda, \quad (28)$$

$$Z' = a \left[C(1-f)^2 + \frac{h}{a} \right] \sin \varphi_g, \quad (29)$$

we can obtain explicit expressions for these three terms as

$$\mathbf{V}_{\dot{\phi}_0}^2 = \dot{\phi}_0^2 a^2 \cos^2 \varphi_g \left(1 + 2f \sin^2 \varphi_g + 2\frac{h}{a} \right), \quad (30)$$

$$\mathbf{V}_{\dot{\phi}_0\dot{\psi}_0}^2 = 2\dot{\phi}_0\dot{\psi}_0a^2 \cos \varphi_g \times \left\{ g + 2f \sin \varphi_g [g \sin \varphi_g + \sin I_0 \sin(\lambda + \phi_0)] + 2g \frac{h}{a} \right\}, \quad (31)$$

$$\mathbf{V}_{\dot{\phi}_0\dot{I}_0}^2 = -\dot{\phi}_0\dot{I}_0a^2 \sin 2\varphi_g \cos(\lambda + \phi_0) \times \left(1 - 2f \cos^2 \varphi_g + 2\frac{h}{a} \right), \quad (32)$$

where we only keep the leading terms of f and h/a and we define the quantity g as

$$g = \cos I_0 \cos \varphi_g - \sin I_0 \sin \varphi_g \sin(\lambda + \phi_0). \quad (33)$$

It can be easily found that the term $\dot{\phi}_0^2 a^2 \cos^2 \varphi_g$ in \mathbf{V}^2 gives the largest contribution due to the rotation of Mars so that

$$\begin{aligned} \frac{1}{2}\mathbf{V}^2 &\approx \frac{1}{2}\dot{\phi}_0^2 a^2 \cos^2 \varphi_g \\ &= 3.22548 \times 10^{-13} \cos^2 \varphi_g, \end{aligned} \quad (34)$$

which is the only term that can reach the level of 10^{-13} for the time transfer. In order to verify this, we define two indicators to show the contribution of the other parts of \mathbf{V}^2 to the time transfer: one is

$$\delta \equiv \frac{1}{2}(\mathbf{V}^2 - \dot{\phi}_0^2 a^2 \cos^2 \varphi_g), \quad (35)$$

and the other is its cumulative contribution in one year

$$\Delta \equiv \int_{T_1}^{T_2} \delta dT, \quad (36)$$

where T_1 is the start time of the lander mission set as 2023 Jan 1; T_2 is the end time set as 2024 Jan 1. Figure 1 shows the color-indexed logarithmic values of $|\delta|$ (left column) and $|\Delta|$ (right column) for the ratio of h/a being -10^{-3} (top panels), 0 (middle panels) and 10^{-3} (bottom panels). It is found that the largest value of $|\delta|$ is at the level of about 10^{-15} and its cumulative contribution in a year is about 10^{-8} s.

Finally, it is necessary to transform the time coordinate of the rotation model from TDB to TCA. Following the IAU 2000 Resolutions, we can have, up to the leading order for the lander (Soffel et al. 2003; Yang et al. 2014),

$$\begin{aligned} \frac{dTCA}{dTDB} &= 1 - \epsilon^2 \left[\frac{\mathbf{v}_{\sigma}^2}{2} + \bar{U}_{\sigma}(\mathbf{x}_{\sigma}) + \mathbf{a}_{\sigma} \cdot \mathbf{X} + \mathbf{v}_{\sigma} \cdot \mathbf{V} \right] \\ &\quad + \mathcal{O}(\epsilon^4). \end{aligned} \quad (37)$$

After a rough estimation, we obtain

$$\frac{dTCA}{dTDB} \approx 1 - 1 \times 10^{-8}. \quad (38)$$

A more detailed investigation on this transformation will be left to our next work. According to IAU 2006 Resolution B3³, it is defined that

$$\frac{dTDB}{dTCB} \approx 1 - 1.5 \times 10^{-8}. \quad (39)$$

Combing them together, we can have an estimation of

$$\frac{dTDB}{dTCA} \approx 1 - 5 \times 10^{-9}, \quad (40)$$

so that the effect of the transformation from TDB to TCA when using Equation (34) is much smaller than 10^{-13} since its leading term is just slightly above this threshold.

3.3 Summary of Internal Contribution

Collecting all terms bigger than the threshold of 10^{-13} for the time transfer, we can write a practical expression for the internal contribution as

$$\begin{aligned} F_{\sigma} &= U_{\sigma}(\mathbf{X}) + \frac{1}{2}\mathbf{V}^2 \\ &\approx \frac{GM_{\sigma}}{a} \left[1 - \frac{h}{a} + \frac{1}{2}J_2(1 - 3\sin^2 \varphi_g) + f \sin^2 \varphi_g \right] \\ &\quad + \frac{1}{2}\dot{\phi}_0^2 a^2 \cos^2 \varphi_g, \end{aligned} \quad (41)$$

which is dominated by the gravitational potential of Mars as a point mass and includes the leading term in the ratio of height to semi-major axis of the areoid h/a , the dynamic form factor J_2 , the flattening f and the spin rate $\dot{\phi}_0$.

4 EXTERNAL CONTRIBUTION

For the external contribution in the time transfer, we mainly follow the approach of Wolf & Petit (1995). Since the distances from the external bodies to the lander are much larger than their characteristic sizes, these bodies can be approximated as point masses up to leading order so that

$$\bar{U}_{\sigma} = \sum_{A \neq \sigma} \frac{GM_A}{r_A}, \quad (42)$$

where M_A is the mass of body A, r_A is the coordinate distance between the lander and the center of mass of body A, and the summation is over all celestial bodies of interest. Therefore, the first three terms in Equation (3) can be expressed as

$$\begin{aligned} \bar{F}_{\bar{U}_{\sigma}} &\equiv \bar{U}_{\sigma}(\mathbf{x}_{\sigma} + \mathbf{X}) - \bar{U}_{\sigma}(\mathbf{x}_{\sigma}) - \mathbf{X} \cdot \nabla \bar{U}_{\sigma}(\mathbf{x}_{\sigma}) \\ &= \sum_{A \neq \sigma} GM_A \left[\frac{1}{r_{LA}} - \frac{1}{r_{\sigma A}} + \frac{\mathbf{X} \cdot \mathbf{r}_{\sigma A}}{r_{\sigma A}^3} \right], \end{aligned} \quad (43)$$

where $\mathbf{r}_{LA} = \mathbf{r}_L - \mathbf{r}_A$ is the vector from body A to the lander and $r_{LA} = |\mathbf{r}_{LA}|$; $\mathbf{r}_{\sigma A} = \mathbf{r}_{\sigma} - \mathbf{r}_A$ is the vector from body A to Mars and $r_{\sigma A} = |\mathbf{r}_{\sigma A}|$. Because of the relation that

$$\mathbf{r}_{LA} = (\mathbf{r}_L - \mathbf{r}_{\sigma}) - (\mathbf{r}_A - \mathbf{r}_{\sigma}) = \mathbf{r}_{\sigma A} + \mathbf{X} + \mathcal{O}(\epsilon^2) \quad (44)$$

³ https://www.iau.org/static/resolutions/IAU2006_Resol3.pdf

Table 4 Values of the Orientation Angles from MRO120D

Parameter	Value	Unit
N	3.37919183	deg
J	24.67682669	deg
ψ_0	81.9683988	deg
$\dot{\psi}_0$	-7608.3	mas yr ⁻¹
I_0	25.1893823	deg
\dot{I}_0	-2.0	mas yr ⁻¹
ϕ_0	133.386277	deg
$\dot{\phi}_0$	350.891985307	deg d ⁻¹

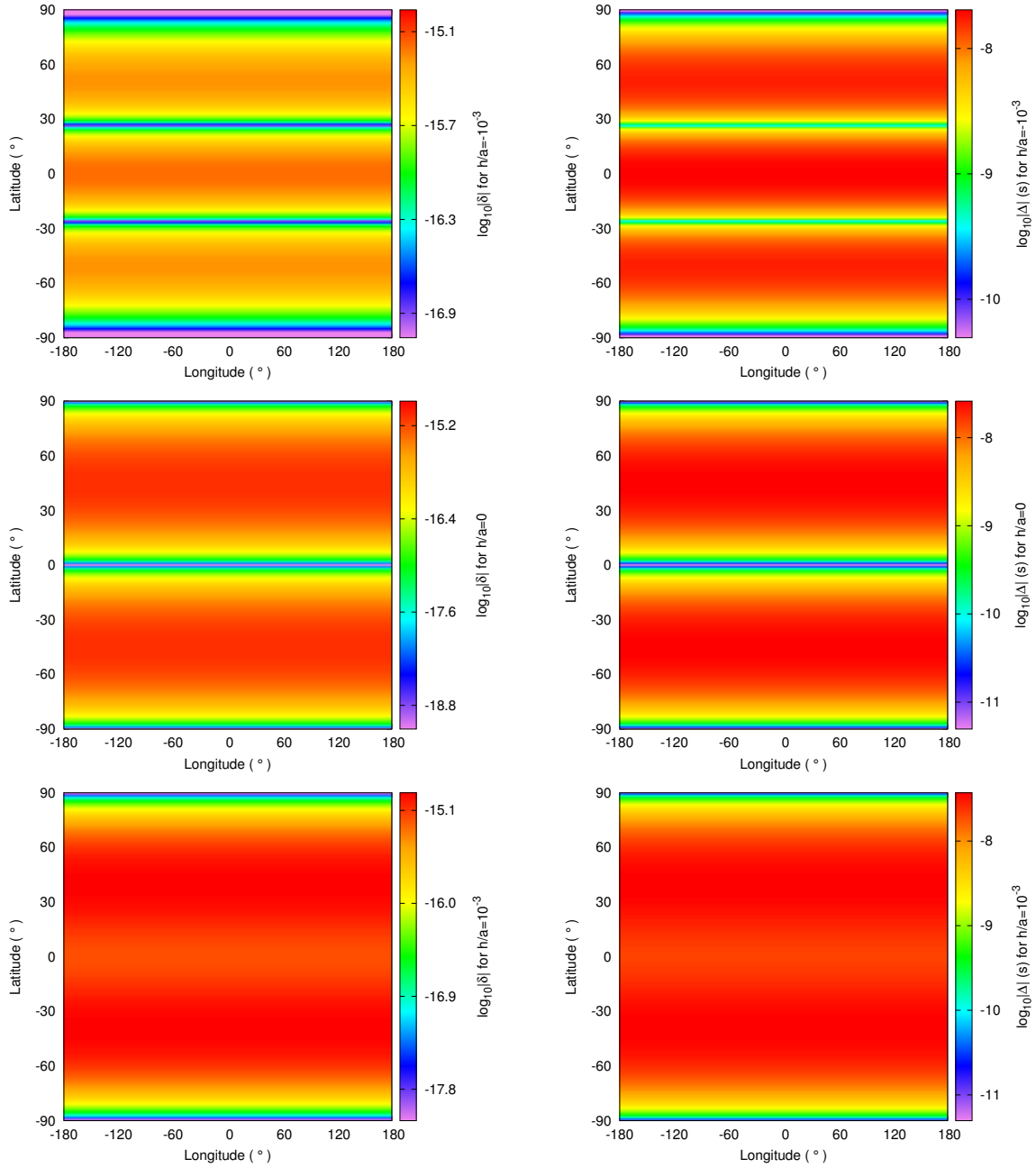
**Fig. 1** Color-indexed logarithmic values of $|\delta|$ and $|\Delta|$ are respectively shown in the left and right columns for the ratio of h/a being -10^{-3} (top panels), 0 (middle panels) and 10^{-3} (bottom panels).

Table 5 Estimation of Maximum Values of $\bar{\mathfrak{F}}_A$, $|\mathbf{Q}_{\sigma^A}|$ and $\epsilon^2 \mathbf{X} \cdot \mathbf{Q}_{\sigma^A}$ for Solar System Bodies

Object	$\max(\bar{\mathfrak{F}}_A)$	$\max(\mathbf{Q}_{\sigma^A}) \text{ (m s}^{-2}\text{)}$	$\max(\epsilon^2 \mathbf{X} \cdot \mathbf{Q}_{\sigma^A})$
Sun	1.2×10^{-18}	3.3×10^{-15}	1.3×10^{-25}
Mercury	4.9×10^{-25}	1.8×10^{-21}	6.7×10^{-32}
Venus	2.0×10^{-23}	1.1×10^{-19}	4.0×10^{-30}
Earth	9.5×10^{-23}	7.1×10^{-19}	2.7×10^{-29}
Mars	—	—	—
Jupiter	8.4×10^{-23}	9.4×10^{-20}	3.5×10^{-30}
Saturn	2.4×10^{-24}	1.2×10^{-21}	4.7×10^{-32}
Uranus	3.4×10^{-26}	8.0×10^{-24}	3.0×10^{-34}
Neptune	9.5×10^{-27}	1.4×10^{-24}	5.2×10^{-35}
Pluto	5.9×10^{-40}	6.4×10^{-38}	2.4×10^{-48}
Ceres	1.1×10^{-27}	3.6×10^{-24}	1.4×10^{-34}
Vesta	1.0×10^{-27}	4.9×10^{-24}	1.8×10^{-34}
Pallas	2.4×10^{-28}	8.0×10^{-25}	3.0×10^{-35}
Phobos	9.4×10^{-20}	6.3×10^{-12}	2.4×10^{-22}
Deimos	8.1×10^{-22}	2.1×10^{-14}	8.0×10^{-25}
“Planet Nine”	3.8×10^{-31}	2.2×10^{-30}	8.6×10^{-41}

and $|\mathbf{X}| \ll |\mathbf{r}_{\sigma^A}|$, we can have

$$\begin{aligned} \frac{1}{r_{\text{LA}}} &= \frac{1}{|\mathbf{r}_{\sigma^A} + \mathbf{X}|} + \mathcal{O}(\epsilon^2) \\ &= \frac{1}{r_{\sigma^A}} - \frac{\mathbf{X} \cdot \mathbf{r}_{\sigma^A}}{r_{\sigma^A}^3} + \frac{1}{2r_{\sigma^A}^3} \left[3 \frac{(\mathbf{X} \cdot \mathbf{r}_{\sigma^A})^2}{r_{\sigma^A}^2} - X^2 \right] \\ &\quad + \mathcal{O}\left(\epsilon^2, \frac{X^3}{r_{\sigma^A}^3}\right), \end{aligned} \quad (45)$$

where we neglect the terms of order higher than X^2 . Substituting the above equation into Equation (43) and using Love numbers k_2 and h_2 to characterize the response of Mars to the tidal potential (the solid Mars tide), we can obtain that

$$\begin{aligned} \bar{F}_{\bar{U}\sigma^A} &= (1 + k_2 - h_2) \times \sum_{A \neq \sigma^A} \left[\frac{GM_A}{2r_{\sigma^A}^3} X^2 \right. \\ &\quad \left. (3 \cos^2 \theta_A - 1) + \mathcal{O}\left(\epsilon^2, \frac{X^3}{r_{\sigma^A}^3}\right) \right] \\ &\leq (1 + k_2 - h_2) \sum_{A \neq \sigma^A} \left[\frac{GM_A}{r_{\sigma^A}^3} X^2 \right. \\ &\quad \left. + \mathcal{O}\left(\epsilon^2, \frac{X^3}{r_{\sigma^A}^3}\right) \right], \end{aligned} \quad (46)$$

where X can be taken as the radius of Mars for the lander and the angle θ_A is defined as

$$\theta_A \equiv \arccos\left(\frac{\mathbf{X} \cdot \mathbf{r}_{\sigma^A}}{X r_{\sigma^A}}\right), \quad (47)$$

and $1 + k_2 - h_2 = 0.86$ (Konopliv et al. 2011).

In order to estimate the contribution of $\bar{F}_{\bar{U}\sigma^A}$ in the time transfer of the lander, we define an indicator for body A in the Solar System as

$$\bar{\mathfrak{F}}_A \equiv (1 + k_2 - h_2) \frac{GM_A}{c^2 r_{\sigma^A}^3} a^2, \quad (48)$$

whose maximum values for the Sun, the other planets (except Mars), Pluto, the three largest main-belt asteroids and the Martian satellites are estimated and listed in the second column of Table 5. In this table, we also include the contribution of a putative trans-Plutonian super-Earth body, also called “Planet Nine,” whose existence is currently a lively debate (Batygin & Brown 2016; Brown & Batygin 2016; Mustill et al. 2016; Iorio 2012, 2014). It is clear that none of them can reach the level of 10^{-13} .

The last term we need to take care of is the last term in Equation (3). The \mathbf{Q}_{σ^A} term is associated with the acceleration of the areocenter in the external gravitational field due to its mass quadrupole. For the Earth, its $|\mathbf{Q}_{\oplus}|$ term is estimated to be on the order of $4 \times 10^{-11} \text{ m s}^{-2}$ due to the Moon (Kopejkin 1991). By making use of equation (22) in Kopejkin (1991), we estimate the maximum values of $|\mathbf{Q}_{\sigma^A}|$ and $\epsilon^2 \mathbf{X} \cdot \mathbf{Q}_{\sigma^A}$ for the lander due to various bodies in the Solar System, and these estimations are listed in the third and fourth columns of Table 5 respectively. As we expect, their contributions in the time transfer are extremely small.

In summary, for the time transfer of the Mars lander from the proper time to TCA, if the threshold of (in)stability is set as 10^{-13} , then all of the contributions from the external bodies can be safely neglected.

5 CONCLUSIONS

Currently, Einstein’s GR has become an inseparable aspect of the procedure for computing time transfer and time synchronization in deep space missions. In the framework of the IAU Resolutions, we investigate the first step in calculating the time transfer for a Mars lander: from its proper time to TCA. From the perspective of practice, we assume that (in)stability of the clock onboard the lander is at the level of 10^{-13} based on facts related to previous deep space missions.

This relativistic time transformation can be divided into two parts: internal and external. The internal one contains the contributions of Mars itself, including its gravitational potential and rotation. Beyond the spherical approximation of Mars, we examine the effects of the non-spherical gravitational potential and the flattened figure of Mars. For the rotation of Mars, we also take the precession, nutation and secular change of Mars obliquity into account. It is found that, for the threshold of 10^{-13} , we only need to keep the following terms: the gravitational potential of spherical Mars and corrections associated with the ratio of the height of the lander on the areoid, the dynamic form factor of Mars, the flattening of the areoid and the spin rate of Mars; see Equation (41) for details.

The external contribution is caused by the external gravitational field of Solar System bodies except Mars. We estimate the maximum components in the external part for the Sun, the other planets (except Mars), Pluto, the three largest main-belt asteroids and the Martian satellites, and find that none of them can reach a level bigger than 10^{-13} ; see Table 5.

Therefore, we can conclude that Equation (41) is sufficiently accurate to describe the relativistic time transfer from the proper time to TCA when the (in)stability of the onboard clock is no better than 10^{-13} . In our next investigations, we will follow the roadmap outlined in Section 1 and work on the transformations from TCA to TCB and from TCA to TCG.

Acknowledgements This work is funded by the National Natural Science Foundation of China (Grant Nos. 11573015 and J1210039) and the Opening Project of Shanghai Key Laboratory of Space Navigation and Position Techniques (Grant No. 14DZ2276100).

References

- Angélil, R., Saha, P., Bondaescu, R., et al. 2014, *Phys. Rev. D*, 89, 064067
- Archinal, B. A., A’Hearn, M. F., Bowell, E., et al. 2011, *Celestial Mechanics and Dynamical Astronomy*, 109, 101
- Batygin, K., & Brown, M. E. 2016, *AJ*, 151, 22
- Brown, M. E., & Batygin, K. 2016, arXiv:1603.05712
- Cacciapuoti, L., & Salomon, C. 2009, *European Physical Journal Special Topics*, 172, 57
- Christophe, B., Andersen, P. H., Anderson, J. D., et al. 2009, *Experimental Astronomy*, 23, 529
- Christophe, B., Spilker, L. J., Anderson, J. D., et al. 2012, *Experimental Astronomy*, 34, 203
- Delva, P., Hees, A., Bertone, S., Richard, E., & Wolf, P. 2015, *Classical and Quantum Gravity*, 32, 232003
- Deng, X.-M. 2012, *RAA (Research in Astronomy and Astrophysics)*, 12, 703
- Deng, X.-M. 2015, *International Journal of Modern Physics D*, 24, 1550056
- Deng, X.-M. 2016, *International Journal of Modern Physics D*, 25, 1650082
- Deng, X.-M., & Xie, Y. 2013a, *RAA (Research in Astronomy and Astrophysics)*, 13, 1225
- Deng, X.-M., & Xie, Y. 2013b, *MNRAS*, 431, 3236
- Deng, X.-M., & Xie, Y. 2014, *RAA (Research in Astronomy and Astrophysics)*, 14, 319
- Dirkx, D., Noomen, R., Visser, P. N. A. M., Bauer, S., & Vermeersen, L. L. A. 2015, *Planet. Space Sci.*, 117, 159
- Dirkx, D., Noomen, R., Visser, P. N. A. M., Gurvits, L. I., & Vermeersen, L. L. A. 2016, *A&A*, 587, A156
- Fountain, G. H., Kusnierkiewicz, D. Y., Hersman, C. B., et al. 2008, *Space Sci. Rev.*, 140, 23
- Genova, A., Goossens, S. J., Lemoine, F. G., et al. 2015, in *EGU General Assembly Conference Abstracts*, 17, 5890
- Genova, A., Goossens, S., Lemoine, F. G., et al. 2016a, in *Lunar and Planetary Science Conference*, 47, 1621
- Genova, A., Goossens, S., Lemoine, F. G., et al. 2016b, *Icarus*, 272, 228
- Hees, A., Folkner, W. M., Jacobson, R. A., & Park, R. S. 2014, *Phys. Rev. D*, 89, 102002
- Hees, A., Lamine, B., Reynaud, S., et al. 2012, *Classical and Quantum Gravity*, 29, 235027
- Hofmann-Wellenhof, B., & Moritz, H. 2005, *Physical Geodesy* (2nd edn.; Berlin: Springer)
- Iorio, L. 2006, *Classical and Quantum Gravity*, 23, 5451
- Iorio, L. 2009, *General Relativity and Gravitation*, 41, 1717
- Iorio, L. 2010, *Central European Journal of Physics*, 8, 509
- Iorio, L. 2012, *Celestial Mechanics and Dynamical Astronomy*, 112, 117
- Iorio, L. 2014, *MNRAS*, 444, L78
- Iorio, L. 2015, *Universe*, 1, 38
- Iorio, L., Lichtenegger, H. I. M., Ruggiero, M. L., & Corda, C. 2011, *Ap&SS*, 331, 351
- Iorio, L., Luca Ruggiero, M., & Corda, C. 2013, *Acta Astronautica*, 91, 141
- Klioner, S. A. 1992, *Celestial Mechanics and Dynamical Astronomy*, 53, 81
- Kliore, A. J., Anderson, J. D., Armstrong, J. W., et al. 2004, *Space Sci. Rev.*, 115, 1
- Konopliv, A. S., Asmar, S. W., Folkner, W. M., et al. 2011, *Icarus*, 211, 401
- Konopliv, A. S., Park, R. S., & Folkner, W. M. 2016, *Icarus*, 274, 253
- Konopliv, A. S., Yoder, C. F., Standish, E. M., Yuan, D.-N., & Sjogren, W. L. 2006, *Icarus*, 182, 23
- Kopejkin, S. M. 1991, *Manuscripta Geodaetica*, 16, 301
- Kouba, J. 2002, *GPS Solutions*, 5, 1
- Kouba, J. 2004, *GPS Solutions*, 8, 170
- Kovalevsky, J., & Seidelmann, P. K. 2004, *Fundamentals of Astrometry* (Cambridge: Cambridge Univ. Press)
- Landau, L. D., & Lifshitz, E. M. 1975, *The Classical Theory of Fields* (4th edn.; Oxford: Pergamon Press)
- Le Poncin-Lafitte, C. 2011, in *SF2A-2011: Proceedings of the Annual Meeting of the French Society of Astronomy and Astrophysics*, eds. G. Alecian, K. Belkacem, R. Samadi, & D. Valls-Gabaud, 669
- Marouf, E. A., Tyler, G. L., & Rosen, P. A. 1986, *Icarus*, 68, 120
- Minazzoli, O., & Chauvineau, B. 2009, *Phys. Rev. D*, 79, 084027
- Misner, C. W., Thorne, K. S., & Wheeler, J. A. 1973, *Gravitation* (San Francisco: W.H. Freeman and Co.)
- Mustill, A. J., Raymond, S. N., & Davies, M. B. 2016, arXiv:1603.07247 (MNRAS in press)
- Nelson, R. A. 2007, in *Frequency Control Symposium, 2007 Joint with the 21st European Frequency and Time Forum*. IEEE International, 1278
- Nelson, R. A. 2011, *Metrologia*, 48, S171
- Oberst, J., Lainey, V., Le Poncin-Lafitte, C., et al. 2012, *Experimental Astronomy*, 34, 243
- Pan, J.-Y., & Xie, Y. 2013, *RAA (Research in Astronomy and Astrophysics)*, 13, 1358

- Pan, J.-Y., & Xie, Y. 2014, RAA (Research in Astronomy and Astrophysics), 14, 233
- Pan, J.-Y., & Xie, Y. 2015, RAA (Research in Astronomy and Astrophysics), 15, 281
- Petit, G., & Wolf, P. 1994, A&A, 286
- Petit, G., & Wolf, P. 1997, IEEE Trans. on Instrum. and Meas., 46, 201
- Petit, G., & Wolf, P. 2005, Metrologia, 42, S138
- Reasenberg, R. D., & King, R. W. 1979, J. Geophys. Res., 84, 6231
- Renzetti, G. 2013, Journal of Astrophysics and Astronomy, 34, 341
- Renzetti, G. 2014a, Ap&SS, 352, 493
- Renzetti, G. 2014b, New Astron., 29, 25
- Renzetti, G. 2015, Acta Astronautica, 113, 164
- Samain, E. 2002, in EGS General Assembly Conference Abstracts, 27, 5808
- Schiller, S., Tino, G. M., Gill, P., et al. 2009, Experimental Astronomy, 23, 573
- Soffel, M., Klioner, S. A., Petit, G., et al. 2003, AJ, 126, 2687
- Torge, W. 1991, Geodesy (2nd edn.; Berlin: W. de Gruyter)
- Turyshchev, S. G., Farr, W., Folkner, W. M., et al. 2010, Experimental Astronomy, 28, 209
- Wolf, P., & Petit, G. 1995, A&A, 304, 653
- Wolf, P., Bordé, C. J., Clairon, A., et al. 2009, Experimental Astronomy, 23, 651
- Xie, Y. 2016, Frontiers in Astronomy and Space Sciences, 3, 15
- Xie, Y., & Huang, Y. 2015, RAA (Research in Astronomy and Astrophysics), 15, 1751
- Yang, Z.-S., Han, Y.-C., Liu, J.-H., et al. 2014, RAA (Research in Astronomy and Astrophysics), 14, 1343
- Zhang, Y.-F., Zhang, X.-Z., Liu, J.-H., Huang, Y., & Xie, Y. 2014, RAA (Research in Astronomy and Astrophysics), 14, 1201